Singular behavior of the neutral modes during directional solidification

J. S. Wettlaufer
Applied Physics Laboratory, HN-10, University of Washington, Seattle, Washington 98105
(Received 22 March 1991; revised manuscript received 17 June 1992)

We study the geometric behavior of the neutral modes of the linearized equations from four directional-solidification models in terms of singularity theory. These equations admit well-known diffusive or Mullins-Sekerka instabilities. For a range of solidification velocity $V_c < V < V_a$, a planar solidification front is linearly unstable to a range of disturbances. The standard neutral curve in linear theory exhibits weak wavelength selection for V near V_c. An equivalence transformation of the neutral-stability relation of the nonsymmetric model distinguishes the basic geometric behavior of this system. The neutral-stability relation is an unfolding of a cubic cuspoid normal form. The solution space of this system is a cusp manifold, generated by families of neutral curves each forming a path in the manifold. This manifold connects two unfolding theories, allowing us to show the sense in which V_c and V_a parametrize degenerate singular points and to show that these points are structurally unstable as critical points. We show that wavelength selection is enhanced in the neutral curves of the transformed system, and that the singularity set of the manifold demarcates stability regions *solely* in terms of control variables. A particular neutral curve will be open or closed depending on how its path crosses the singularity set, and the system will not admit hysteresis. The weak wavelength selection is due not only to the thermophysical or control parameters of the material, but to the singular behavior that is intrinsic to the formulation. We show that four solidification models possess cubic normal forms, and that asymptotic limits reveal two different normal forms. The main goal is to point out the geometric structure of a model, and to show how one can distinguish different solidification formulations and asymptotic limits, using simple geometric criteria.

PACS number(s): 81.10.Dn, 81.30.Fb, 47.20.Hw, 47.20.Ky

I. INTRODUCTION

The directional-solidification system [1] is used in a number of forms to examine the unidirectional solidification of binary alloys, and has been studied because of its wide practical interest and intrinsic mathematical behavior. The alloy is pulled with a constant speed V through an imposed thermal field, and a mean position is established at which the planar solid-liquid interface is located. A phase boundary will remain planar if the stabilizing influences of the thermal fields and surface tension suppress the destabilizing effects of solute rejection at the interface [2,3]. This state can be maintained for growth velocities V less than a critical velocity V_c or above a velocity V_a. When $V = V_c$, there is a bifurcation to a cellular phase boundary. The physics of this process is generic, in that any pure solid that is solidifying from a binary melt has an unstable phase boundary for growth velocities above the threshold V_c, where the solute diffusion process is too slow to remove local solutal undercooling. The classical analysis of Mullins and Sekerka [2] identified these limits for an alloy solidifying in a constant temperature gradient.

We consider solidification in which the system is infinite in the direction perpendicular to the mean motion of the interface. Therefore, the system width is not a control parameter, as is commonly the case [4,6]. The stability of the system is examined by introducing an interfacial disturbance of the form $\exp(\sigma t + iax)$, where σ is the complex growth rate, and a is a wave number in the direction x, perpendicular to the mean growth direction. Initially we focus on the thermally nonsymmetric (thermal conductivities of both phases differ), chemically one-sided (solute diffusion in the solid is negligible) model. This distinction is important, since analyses of symmetric models are not readily comparable to one-sided models [5]. In thermally symmetric, zero-latent-heat models (e.g., [3]) interfacial disturbances do not induce disturbances in the thermal fields; the temperature gradient across the entire solid-liquid system is constant. Here, the effect of the latent heat liberated at the interface is accounted for, and convective transport of heat or solute is proscribed (Fig. 1). The length and time scales are based on the solute diffusion scales D/V and D/V^2, respectively, where D is the solute diffusivity in the liquid. The advantage of this scaling is that standard dimensionless control parameters M, the morphological number, which is a measure of the degree of constitutional undercooling, and Γ, the surface-tension parameter, will result when the thermal and solute fields are suitably scaled. A disadvantage is that both control parameters depend on the planar growth velocity V and the far-field solute concentration C_∞. By weak wavelength selection for a system [6], it is meant that V_c, for the onset of instability, depends weakly on the disturbance wavelength. This is one of the difficulties in comparing the standard theory [1–3] with experiment, and results in a strong interaction between short- and long-wave disturbances above V_c [6]. The absence of horizontal boundary conditions results in normal modes that depend continuously

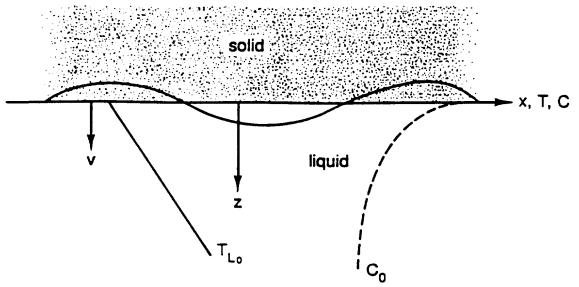

FIG. 1. Schematic of the solidification system in which the phase boundary is moving downward into the liquid. The steady-state thermal T_{L0} and concentration C_0 fields are represented, and there are no horizontal boundaries.

on wave number, which may to some extent result in this selection mechanism. Constraining the horizontal dimension results in a discretized spectrum, limiting mode interaction [4,6]. When the system width is used as an additional control parameter, the dimensionality of the problem is effectively increased.

Linear theory provides a characteristic equation relating the disturbance growth rate σ to wavelength, mean growth velocity, and other control variables: $F(\sigma,a,M(V,C_\infty),\Gamma(V,C_\infty),\text{controls})$. For direct steady modes, setting $\sigma=0$ demarcates between stability and instability, the boundary being defined by a neutral stability relation $g(a,M,\Gamma,\text{controls})=F(\sigma=0,,,,)$. Solving the bifurcation problem for g allows the construction of two neutral curves that are of particular interest: $V(C_\infty)$ and $V(\lambda)$, where λ is the dimensional wavelength of the disturbance.

A particular coordinate transformation on g yields a more useful function of control parameters $f(x,\alpha,\beta)$, where x represents wave number and α and β represent the controls. The solution space of the system is a cusp manifold, generated by families of neutral curves f_k each forming a path in the manifold. We view f as a one-parameter unfolding (Sec. III) of a cuspoid normal form $N=x^m$, $m=3$. The cusp manifold is defined by f_2, a two-parameter unfolding of N. This manifold connects two unfolding theories, allowing us to show the sense in which V_c and V_a parametrize degenerate singular points, and that these points are structurally unstable as critical points. We find that the manner in which a path intersects the bifurcation set of f_2 determines the structure of a neutral curve, and that steady solutions admit no hysteresis. At neutral stability, we find that three other solidification models are represented by unfoldings of a cubic normal form, and that in certain short- and long-wave asymptotic limits, the normal form is either a quadratic or quartic cuspoid. By comparing the nonsymmetric model to one based on different length and time scales, we find that the flatness of the neutral curve is due to both the control parameters thermophysical properties of the material *and* the intrinsic structure of the normal form. Thus we view the standard neutral curves in a different manner, one which has basic geometric significance.

In the next section a Mullins-Sekerka instability for this system is formulated, and we draw a standard neutral curve $V(\lambda)$. In Sec. III we examine the cusp manifold determined from $f_2=0$, and a path of f. We show the condition that dictates the closedness of the neutral curve, and that V_c and V_a parametrize degenerate critical points that are unstable as critical points. We present the geometric criteria that distinguishes between solidification formulations and their asymptotic limits. We point out the origin of the wavelength selection problem and, in Appendix A, we show the link between two unfolding theories in the case of one state variable. The results apply to any binary alloy for which these solidification models are valid.

II. FORMULATION

The system [1,2] is a continuum description of heat and mass transfer, so the basic ingredients are the diffusion fields through both phases. The reference frame is attached to the solidification front which is moving with a speed V into the liquid (Fig. 1). The lengths and times in the problem are scaled on the solute diffusion scales $z,x=(z',x')V/D$ and $t=t'V^2/D$, where the primed quantities have dimensions. The temperature T and solute C scales are

$$T_{L,S}=\frac{T'_{L,S}-T'_0}{G^*D/V}\ , \tag{1}$$

$$C=\frac{C'k-C_\infty}{(k-1)C_\infty}\ , \tag{2}$$

where the subscripts L,S denote the liquid and solid phases, and T'_0 is the reference temperature of the planar interface. The dimensional temperatures $T'_{L,S}=T^*_{L,S}-T_m$ are measured relative to bulk melting temperature T_m of the pure substance. These are related to the scales from a thermally symmetric, zero latent heat analysis [7], but here we include latent heat. The quantity $G^*=(2G'_L+LV/k_l)/(1+n)$ is the average temperature gradient at the planar interface. The dimensional temperature gradient in the liquid is G'_L, the latent heat per unit volume is L, and the ratio of the thermal conductivity of the solid to that of the liquid is $n=k_s/k_l$. The far-field solute concentration is C_∞, and k is the segregation coefficient, giving the ratio of the solute in the solid to that in the liquid. We consider k to be less than unity, representing the low solubility of impurity in the solid.

Using the above scales, the dimensionless diffusion fields obey the following two-dimensional equations and boundary conditions. For the liquid, $z>h(x,t)$,

$$\nabla^2 T_L=0\ , \tag{3a}$$

$$\nabla^2 C+C_z=C_t\ ; \tag{3b}$$

for the solid, $z<h(x,t)$,

$$\nabla^2 T_S=0\ . \tag{3c}$$

At $z=h(x,t)$,

$$T_L=T_S=MC+M\Gamma h_{xx}(1+h_x^2)^{-3/2}\ , \tag{4}$$

$$l(1+h_t)=n(T_{Sz}-h_xT_{Sx})-(T_{Lz}-h_xT_{Lx})\ , \tag{5}$$

$$(1+h_t)[1+C(k-1)]=C_z-h_xC_x\ . \tag{6}$$

In the far field,

$$T_L\to T_{L0},\quad C\to C_0\ \text{ as } z\to\infty\ , \tag{7}$$

$$T_S\to T_{S0}\ \text{ as } z\to-\infty\ , \tag{8}$$

where the subscripts x,z,t denote partial differentiation. Equations (3a) and (3c) represent the limit as D/κ_L and D/κ_S approach zero, where κ_L (κ_S) is the thermal diffusivity of the liquid (solid). Condition (4) is an impurity corrected Gibbs-Thomson relation. The latent heat parameter appearing in condition (5) is $l=LV/k_lG^*$. Far from the interface the influence of the deflection $h(x,t)$ on the diffusion fields will be negligible, so the steady-state planar solutions T_{L0}, C_0, and T_{S0} will adequately describe them. The morphological number M and surface tension parameter Γ are the standard nondimensional parameters appearing in (4),

$$M=\frac{mG_c}{G^*}=\frac{mC_\infty(k-1)V}{DkG^*}\ , \tag{9}$$

$$\Gamma=\frac{T_m\gamma_{sl}kV}{LDmC_\infty(k-1)}\ , \tag{10}$$

in which m is the liquidus slope, taken from a locally linear binary phase diagram. The steady-state solute gradient at the interface is G_c, and γ_{sl} is the solid-liquid interfacial surface tension. It is important to recognize that in this formulation the velocity dependence of M is also implicitly represented in G^*, which is not the case in a model without latent heat. Equations (3)–(8) completely describe the mathematical problem for the unknown functions C, T_L, T_S, and h.

The basic states, which represent the planar interface, are perturbed as $z=h(x,t)=\exp(\sigma t+iax)$, and we keep track of their temporal behavior. When solving the resulting eigenvalue problem for the growth rate σ using a standard procedure (e.g., [1–3]), a characteristic equation, that is an implicit function of σ is obtained,

$$\sigma=\frac{a[M\hat{R}(1+n)-(2G_L+l)(\hat{R}+k)-a^2M\Gamma(\hat{R}+k)(1+n)]}{l(\hat{R}+k)+Ma(1+n)}\ , \tag{11}$$

in which $\hat{R}=(\frac{1}{4}+a^2+\sigma)^{1/2}-\frac{1}{2}$ is a wave-number parameter. If $\mathrm{Re}(\sigma)=0$, then $\mathrm{Im}(\sigma)=0$, since there is an exchange of stabilities for the finite-latent-heat system [8]. When $\mathrm{Re}(\sigma)>0$ the planar interface loses stability to nonoscillatory or direct disturbances, and when $\mathrm{Re}(\sigma)<0$ it is stable. By setting $\sigma=0$, we obtain the condition that must be satisfied by the neutrally stable modes,

$$R^3+R^2(1+k)+\frac{R}{\Gamma}\left[k\Gamma+\frac{1}{M}-1\right]+\frac{k}{M\Gamma}=0\ , \tag{12}$$

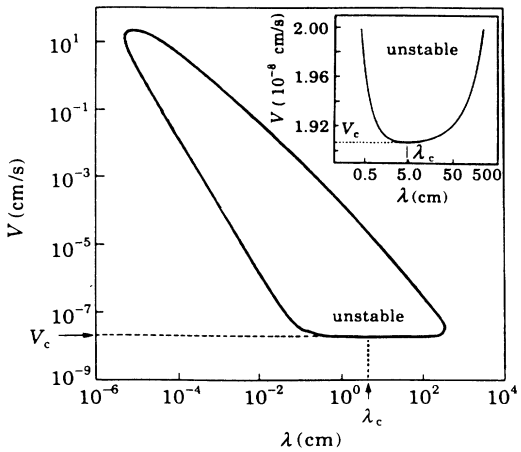

FIG. 2. The dimensional $V(\lambda)$ neutral-stability curve for an H_2O-NaCl system [10] with $C_\infty=0.035$ wt.%, $n=3.57$, $k=0.3$, $G_L'=3.57$ K m^{-1}, $\gamma_{sl}=33$ mJ m^{-2}, and $L=3.06\times10^8$ J m^{-3}. The planar interface is unstable interior to the curve. The inset is the neutral curve near the critical velocity, $V_c(\lambda_c)$.

where $R=\hat{R}(\sigma=0)$. This is the neutral function g referred to earlier, and can be transformed to the cubic obtained by Coriell, McFadden, and Sekerka [9], who used different temperature and solute field scalings. The locus of points $(R>0,M,\Gamma)$, for a given segregation coefficient k, demarcates regions of stability from regions of instability, since $\sigma=0$ at every point satisfying Eq. (12).

We use Eq. (12) to draw a dimensional neutral stability curve in the (V,λ) plane, for the material parameters of an H_2O-NaCl system [10]. Figure 2 shows the entire neutral curve, and the inset shows the bottom of the neutral curve close to V_c. Near the critical velocity, we see the weak dependence of V on λ noted by other investigators, e.g., [6,11]. There are short (due to surface tension) and long (due to the finite interaction range of the solute field) λ cutoffs which bound the allowable scale of the interfacial substructure.

III. SURFACE OF NEUTRAL STABILITY

We examine the neutral modes determined from Eq. (12), and the analogous expressions from other models, within the framework of singularity and catastrophe theory [12,14,15]. The purpose is to obtain a geometric interpretation of systems behavior, extending previous discussions [9] of this result. In this section we will see (a) the topological origin of the wavelength selection problem within this system of equations; (b) that even in physical systems in which weak wavelength selection is a prominent feature of the linear analysis, the selection is enhanced when transforming solutions into a different neutral surface; (c) the sense in which V_c and V_a parametrize degenerate singular points, and that these

points are structurally unstable as critical points; (d) that the topological behavior is intrinsic to the formulation, and independent of the physical scaling chosen; and (e) that we can distinguish between different solidification formulations *and* asymptotic regimes of the same system by studying the number and nature of the critical points.

A. Relation to cubic cuspoids

A *bifurcation diagram* is defined by the set (x,ξ_0) that satisfies a scalar equation of the form $g(x,\xi_0)=0$, in which x is the unknown state variable, and ξ_0 is the *bifurcation parameter.* Singularity theory [12] deals with the conditions under which two such equations and their bifurcation diagrams are qualitatively similar. Appendix A outlines these conditions. Typically, the state variable will represent the solution amplitude of a set of differential equations put in one-to-one correspondence with the above scalar system via Liapunov-Schmidt reduction. Locally, this procedure puts the solutions to a system of n equations (n can be infinite) in one-to-one correspondence with the solutions of a k-parameter family of bifurcation problems, $g(x,\xi)=0$, where $\xi=(\xi_0,\ldots,\xi_k)$. Generally, we think of ξ_0 as the bifurcation parameter, and $\xi_1,\ldots,\xi_k$ as auxiliary parameters. For the thermally symmetric system, placed in a small periodic box, Haug [4] investigated the variation of the disturbance *amplitudes* with bifurcation parameter V, allowing only single and two-mode bifurcations. He restricted k and n to values near unity, and used symmetry arguments to identify possible normal forms, but did not show when they occur. Here, x represents *wave number* rather than amplitude.

We can write Eq. (12) as

$$g=R^3+pR^2+qR+r=0\ , \tag{13}$$

where the form of the coefficients can be obtained by inspection. g is a monotonically increasing function of R for all k,M,Γ when $q>0$, since p and r are always positive. [For the thermally symmetric system, a (k,M,Γ) surface has been examined; first Ref. in [13]]. We remove the quadratic term by performing the transformation $R=x-p/3$, giving the bifurcation problem that defines the neutral path mentioned above,

$$f=x^3+\alpha x+\beta=0\ , \tag{14}$$

where α and β depend on the underlying control parameters V, C_∞, G_L', k, etc. The qualitative features of the bifurcation problems for f and g do not change under this equivalence transformation. The function f is a universal unfolding (in the sense of contact equivalence [12]) of the cubic cuspoid normal form $N=x^3$, and has been studied in the context of singularity and bifurcation theory [12]. It is necessary to consider two unfoldings of N: f as in Eq. (14) and $f_2(x,A,B)$, a two-parameter unfolding,

$$f_2=x^3+Ax+B=0\ , \tag{15}$$

in which A and B are not slaved to one control parameter, but can attain all control states accessible to the solidification system. We define the bifurcation diagram

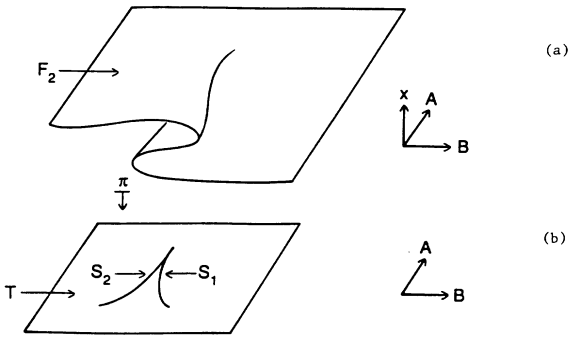

FIG. 3. (a) The *neutral surface* F_2; a two-parameter unfolding (with respect to contact equivalence [12]) of the cuspoid normal form x^3. (b) The projection π of the surface onto the control plane $T(A,B)$ where the cusp forms the *bifurcation set S,* with right- and left-hand nappes S_1 and S_2, respectively. Inside the cusp there are three real solutions to $f_2=0$, and outside there is one.

$F_2=\{(x,A,B):f_2=0\}$ as the *neutral surface* since everywhere on the surface the base states are neutrally stable. This surface is shown in Fig. 3(a).

The sheets of the surface illustrate the root structure of (15). In Fig. 3(b) the points of F_2 are projected onto the plane of control parameters $T(A,B)$,

$$\pi\colon F_2\mapsto T \Longleftarrow (x,A,B)\mapsto(A,B)\ .$$

The points that satisfy $f_2=\partial_x f_2=0$ are given by the equation

$$D=4A^3+27B^2=0\ , \tag{16}$$

defining the *bifurcation set S* of (15), where the tangent plane to the neutral surface is perpendicular to the control plane [12,14]. So, the projections of the folds in F_2 into T are the folds in T, defined by S. As (A,B) pass through S, into the interior of the cusp region [Fig. 3(b)], the root structure of (15) changes from one real and two complex conjugate roots, to three real roots. Two real roots meet along S, and three real roots meet at the cusp point $A=B=0$. Looking up in the x direction from a point $T(A',B')$, one might see three layers of the surface F_2, or just one, corresponding to the number of points in F_2 with control state (A',B'). $f_2=\partial_x f_2=0$ along $D=0$, so Eq. (16) generates a set of *degenerate singular* points [12,14]. The qualitative nature of the system will change *only* when the bifurcation set is crossed.

A useful treatment of the solidification system is to use V as the bifurcation parameter, and fix auxiliary parameters C_∞, k, etc. $f(x,\alpha,\beta)$ is a one-parameter unfolding of N, where $(\alpha,\beta)\subset(A,B)$ both depend on V. We define the bifurcation diagram $F=\{(x,\alpha,\beta):f=0\}$ as the *neutral path* since everywhere along this path the base states are neutrally stable. Thus F_2 is a surface; A and B vary independently, and F is a subset of the surface that can be formed using (α,β) in $T(A,B)$. F is a closed set, determined by the range of growth velocity that is physically accessible to a system with fixed auxiliary parameters, so there are only a finite number of points where F meets S.

The closedness of a neutral curve, defined by $F \cap F_2$, depends on this number. Since $(\alpha,\beta) \subset (A,B)$, then $F \cap F_2 = F$, so that in practice one focuses on F. For fixed auxiliary parameters, F is the only path accessible to a particular system. A slice of the fold region at constant x will give the standard $C_\infty(V)$ neutral curve. By varying an auxiliary parameter, say C_∞, we can obtain a family of paths F_k in F_2. Golubitsky and Schaeffer [12] prove that the universal unfoldings of all bifurcation problems $G(x, A, B)$, in one state variable x, and of finite codimension, that satisfy $G(x,0,0) = x^3$, may be written as parametrized families of paths through the cusp.

Now we investigate the qualitative behavior of this solidification formulation by examining a path. The physical controls are the values of α and β that can be obtained by varying V through the same range as in Fig. 2. In Fig. 4, we show the neutral path of the H_2O-NaCl system from $V < V_c \Longleftrightarrow (\alpha > \alpha_c, \beta > \beta_c)$, to $V > V_a \Longleftrightarrow (\alpha > \alpha_a, \beta < \beta_a)$, in both the surface F_2 [Fig. 4(a)] and in the control plane T [Fig. 4(b)]. We can think of the bifurcation diagram (here, a neutral curve) as what is recovered by lifting the path in T to the cusp surface F_2. The path begins at $(\alpha > \alpha_c, \beta > \beta_c)$ on the right-hand sheet where $x < 0$, so the solutions are unphysical there. At critical $(\alpha,\beta) = (\alpha_c,\beta_c)$, the path jumps up to the right-hand fold where the tangent plane is perpendicular to the control plane. The upper fold in the pleated region is the only fold of physical interest since $x > p/3$ is required for positive wave numbers. After passing through the initial bifurcation point of the path (x_c,α_c,β_c), the roots split. If $\beta < 0$ in the pleated region, the neutral curve would break since $x \leq p/3$ is not allowed. Finally, as $\alpha \to \alpha_a$ and $\beta \to \beta_a$ the roots coalesce at $x = x_a$, closing the neutral surface (and curve). The system restabilizes when the path exits the pleated region through the right-hand nappe S_1, of the bifurcation set S, through which it entered. Thus, if a neutral path enters the cusp region by crossing through S_1, then in order for the neutral curve to be closed it must exit through S_1. The curve will be open if the neutral path exits through S_2. We can see this by taking a slice of F_2 at constant A and moving B through $B = 0$ and S_2 as shown in path a of Fig. 5. The path runs off on the upper left-hand sheet leaving a single branch to the neutral curve. In this case, there is no restabilization of the planar interface. Since unphysical solutions exist on the lower fold, there is no hysteresis associated with the critical points. Two other paths and their bifurcation diagrams are shown in Fig. 5. In path c of Fig. 5 we see an island, or isola, of unphysical stationary states, unconnected to the physical branch. Isolas have also been seen in the amplitude bifurcation diagrams [4,11]. If the system were formulated in such a way that only negative wave numbers were allowed, then a neutral curve would be closed when the path entered and exited through the left-hand nappe as shown in path c of Fig. 5.

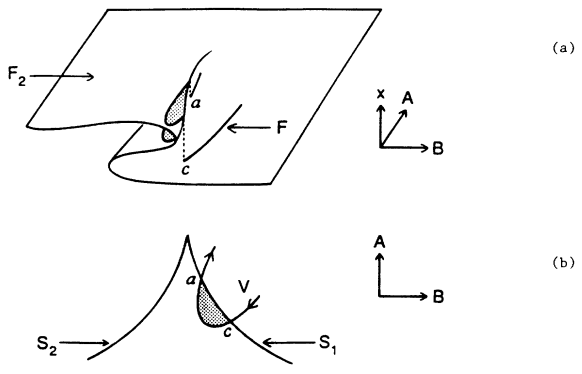

FIG. 4. (a) The *neutral path* F in the surface F_2. The path "begins" on the lower right-hand sheet of F_2 where the solutions are unphysical. The path "jumps" up to the right-hand fold [see (a)] or crosses the right-hand nappe of the *bifurcation set* S_1 [see (b)] when $(A,B) = (\alpha_c,\beta_c)$, labeled by c. The system stabilizes after exiting the cusp region [see (b)] at $(A,B) = (\alpha_a,\beta_a)$, labeled by a. The shaded area is the region of instability. The path is parametrized by the underlying bifurcation parameter V, and C_∞ is fixed at the value in Fig. 2. A neutral curve is closed if the path F enters and exits S by crossing S_1.

In the symmetric model of solidification [3], sufficiently long wavelengths are unstable, resulting in an open neutral curve. Here we see the geometric distinction (as opposited to those discussed in [5]) between the symmetric and nonsymmetric formulations. The bifurcation at (x_c,α_c,β_c) is not equivalent to the pitchfork normal form $x^3 + \alpha x = 0 (\alpha < 0)$, and cannot be considered as a perturbation of the pitchfork since $\beta_c \gg 0$. Here, the neutral path crosses the bifurcation set twice, resulting in a closed neutral curve with two critical points. The curve is closed because the same nappe of the bifurcation set is crossed. We discuss the stability of the critical points in the next section.

Near critical, the α-x neutral curve is *relatively* sharper than the β-x neutral curve. In part, this behavior is due to the velocity dependences of α and β; $\partial|\alpha|/\partial V > \partial\beta/\partial V \gg \partial M/\partial V$. In Fig. 6 the $|\alpha|$-x and β-x neutral curves are superposed. Both curves are closed since the path leaves the folded region by passing through S_1. Relative to the standard neutral curve close to the critical velocity, the $|\alpha|$-x curve exhibits strong wave-

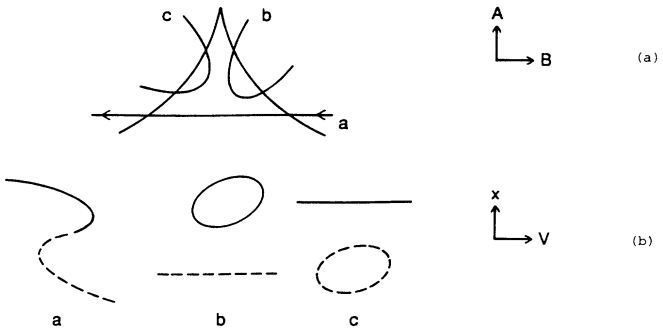

FIG. 5. (a) Three paths through the *bifurcation set* S in T and (b) their associated bifurcation diagrams. The horizontal coordinate is the underlying bifurcation parameter V, and the dashed lines refer to unphysical solutions. The direction of path a is discussed in the text. The neutral curve is open for path a and path c. Path b is similar to F.

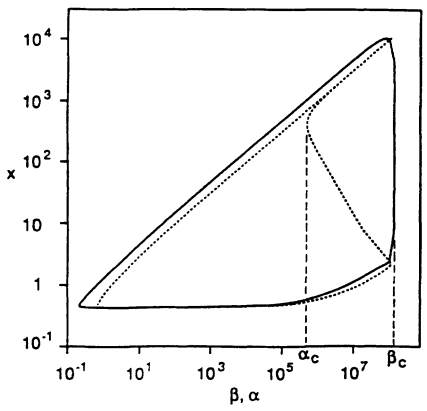

FIG. 6. The $|\alpha|(x)$ (dotted line) and $\beta(x)$ (solid line) neutral curves from $(A,B)=(\alpha_c,\beta_c)$ to $(A,B)=(\alpha_a,\beta_a)$. There is *relatively* strong wavelength selection in the $|\alpha|(x)$ plane due to the dependence on V, and $\beta(x)$ resembles the standard curve near the critical velocity.

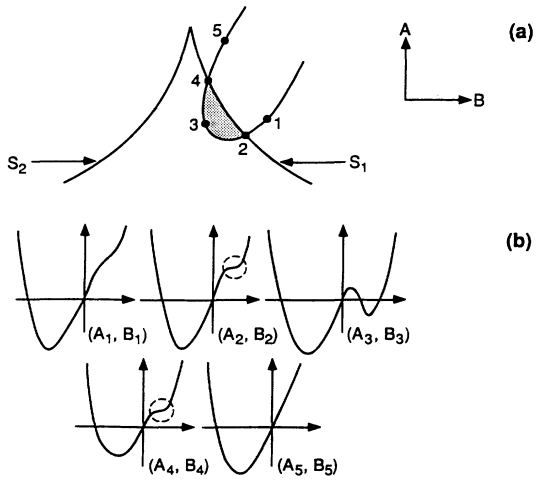

FIG. 7. (a) Five points (A_i,B_i) in F. (b) The graph of $\Phi(x,A,B)$, an unfolding (with respect to right equivalence [12]) of the cuspoid normal form x^4 for these five points. We are particularly interested in the structure of the critical points. Notice (dashed circle) that at the points (A_2,B_2) and (A_4,B_4), the function Φ has locally cubic inflections. These singularities correspond to velocities V_c and V_a, and are structurally unstable as critical points, and the equilibria of Φ form the surface F_2 in Fig. 3 (see text).

length selection, and folds back over itself on this scale. The β-x curve exhibits *relatively* weak wavelength selection near the critical velocity, and the curves are qualitatively similar for values of $|\alpha|,\beta<10^5$. The $|\alpha|$-x curve is more interesting close to the critical velocity because α is changing very rapidly, but β undergoes very little change for x ranging over more than two orders of magnitude. Since $|\alpha|$ reaches a maximum after the critical value and then turns around to approach α_a [Fig. 4(b)], the critical wave number is flanked by bands of unstable modes, which are themselves flanked by upper and lower cutoffs. The upper and lower cutoffs are the surface-tension and finite-solute-diffusion-range stability limits, but the intermediate bands are a result of the turnaround of α, giving a quartic structure to the curve. The relatively flat β-x curve stems from the fact that the critical point occurs on a part of the upper fold with small curvature. Together, these curves display the topological origin of the weak wavelength selection observed in a standard neutral curve, and we return to this in Sec. III D.

B. Relation to quartic cuspoids

When there is only one state variable, the unfoldings of normal forms in singularity theory are simply related to those of catastrophe theory [12]. The theories differ in the definition of the *equivalence* of two functions, but the pictures generated are the same. We can think of F_2 as the singularity set of a generating function $\Phi(x,A,B)=\frac{1}{4}x^4+(A/2)x^2+Bx$, an unfolding (with respect to right equivalence [12]) of the cuspoid $\phi(x)=\frac{1}{4}x^4$. In the language of catastrophe theory $\phi(x)$ is the *cusp catastrophe,* whereas in singularity theory the cusp catastrophe is the universal unfolding (in the sense of contact equivalence [12]) of x^3 The catastrophe manifold determined from $\partial_x\Phi=0$ is identical to the surface in Fig. 3. $\phi(x)$ does not degenerate under perturbations of either the generating function or the catastrophe manifold [14,15], so we can focus on either, with no loss in generality.

We ask what $\Phi(x,A,B)$ looks like for the five points (A_i,B_i) in T, shown in Fig. 7(a), and graph $\Phi(x,A,B)$ for these points in Fig. 7(b). We are particularly interested in the structure of the critical points. At 1, Φ has one relative minimum. At 2, the critical point associated with V_c, an inflection is created, accompanying the existing relative minimum. Inside S, at 3, Φ has two relative minimum and a maximum. At 4, associated with V_a, the right-hand minimum and maximum coalesce to form another inflection. One relative minimum returns at 5. Since the neutral states of the system exist on a manifold that minimizes Φ, we view Φ as a potential. The minima of Φ correspond to stable equilibria, and the maxima and inflections correspond to unstable equilibria.

The inflection points are locally cubic x^3 [dashed circles in Fig. 7(b)]. Consider point 2, associated with V_c. In a standard experiment it is desirable to operate with $|1-V/V_c|\ll 1$, so we investigate the stability of this critical point with respect to disturbances in V. A perturbation of x^3 by ϵx, where $|\epsilon|\ll 1$, can arise from small variations in the mean solidification velocity δV, due to fluctuations in the experimental control temperatures. Thus, when $|1-V/V_c|\ll 1$, $\epsilon=\delta A$ or δB, where $\delta V>0$ is equivalent to $\epsilon<0$, and $\delta V<0$ is equivalent to $\epsilon>0$. When $\epsilon>0$ there are no critical points, corresponding to the transition from 2 to 1. When $\epsilon<0$ there are two, a minimum and a maximum, corresponding to a transition from 2 to 3. The same argument can be applied to point 4, associated with V_a. Therefore, the critical points of the solidification system correspond to points of Φ that are structurally unstable *as critical points;* they degenerate into two critical points or zero. When the degree n

increases, x^n behaves worse in this respect [14]. For example, if x^4 is perturbed by ϵx^2, it either becomes a single minimum $\epsilon > 0$, or two minima and a maximum $\epsilon < 0$. However, x^2 is structurally stable against perturbations by ϵ. This is an important point if, for example, the neutral function f, as in (14), is an unfolding of a quartic normal form. It is tempting to simply investigate the dependence of the variable $y = x^2$ with control parameters (e.g., Eq. (4.5), third Ref. in [13]). One must proceed with caution, because it is possible that the generic stability behavior of the system will be lost, for example, masking the singular behavior of a quartic with that of a quadratic. Related examples are presented in the next section.

C. Relation to other models and asymptotic normal forms

Thermally symmetric or frozen-field models assume that $\kappa_L = \kappa_S$, and that $l = LV/k_l G^* \ll 1$, the latter approximation being poor at high growth speeds [3]. In this case, linear perturbation theory gives a neutral surface that is an unfolding of a cubic normal form, with unfolding parameters that depend differently on the bifurcation parameter. Asymptotic behavior reveals several distinct normal forms.

Long-wave phenomena are of interest because they are accompanied by long time scales, or slow modes of evolution. The long-wave limit has been examined in the absolute stability and constitutional undercooling-small k regions of parameter space of this system [13]. Riley and Davis [13] review the former two analyses and examine the long-wave behavior for small k, and large Γ, and for small k near absolute stability, to exhaust the possibilities for the frozen-field system in which solute is rejected ($k < 1$).

Near the critical velocity, Sivashinsky [13] defined a small parameter $\epsilon = 1 - M^{-1}$, and investigated the long-wave behavior in the limit $k \ll a^2 \ll 1$. This limit dictates new length and time scales. When rescaling the frozen-field equations, and performing linear stability analysis, the resulting neutral surface is an unfolding of a quartic normal form,

$$x^4 + c_1 x^2 + c_2 = 0 \ . \tag{17}$$

This expression follows from Sivashinsky's Eq. (20) [13], where the c_i are the unfolding parameters containing the controls, and x is a wave number.

Near absolute stability, Brattkus and Davis [13] chose $\epsilon = k^{-1} - \Gamma$ as a small parameter, and investigated the long-wave limit $a^2 \ll 1 \sim k$. After rescaling the solidification equations, linear stability analysis yielded a neutral surface of the same form as Eq. (17) above, which follows from their Eq. (4.5). We note that although the nonlinear evolution equations developed in these two long-wave limits behave differently, the unfolded normal forms possess the same geometric structure. The unfolding parameters c_i are presented in Appendix B.

When applying the short-wave limit $a^2 \gg 1 \gg k$ to Eq. (12), for arbitrary values of other parameters, the neutral surface is the unfolding

$$x^2 - c_1' + c_2' = 0 \tag{18}$$

of a codimension one normal form $x^2 - c_1'$, known as the *simple bifurcation* [12].

In a model of rapid solidification [7] with zero latent heat, velocity dependent segregation and liquidus slope, and linear attachment kinetics, linear perturbation theory yields a neutral surface that is the unfolding of a cubic normal form as in Eq. (14). One can derive this expression by choosing a wave number in Eq. 4.2(a) of [7(a)] or Eq. 3.5(a) of [7(b)] that is related to R or x here (see Appendix B). In the former case let $\lambda_1 = -\lambda_1$; in the latter case, let λ_1 be the wave number, and remove the quadratic terms when $\sigma = 0$. Asymptotic analysis of this system will also reveal noncubic normal forms. As one might expect, purely chemical or thermal solidification systems result in different normal forms [3]. Therefore, we can distinguish between asymptotic limits of a given solidification system, and between different formulations, by the degree of the normal form, and the number of unfolding parameters. This provides a classification based on the number and nature of a systems critical points, and allows one to ask, "When are two solidification systems, or asymptotic limits of a particular system, qualitatively similar?" At this point, we know that the thermally nonsymmetric finite latent heat system, the frozen-field system, and one model for rapid solidification, have a neutral surface that is a two parameter unfolding of a cubic cuspoid normal form, and that particular long- and short-wave limits have quartic and quadratic normal forms. These are summarized in Table I.

D. Wavelength selection

Weak wavelength selection is commonly explained as the result of the small values of solid-liquid surface tension in the material systems studied [6]. Indeed typical values of the capillary length γ_{sl}/L (tabulated in [16]) are of the order of a few angstroms, providing a cutoff for the stabilization of short-wave disturbances. However, the flatness of the neutral curve admits the interpretation

TABLE I. Unfolded normal forms for four solidification models and three asymptotic limits.

Model	Asymptotic limit	Unfolded normal form	Codimension
Nonsymmetric	Nonasymptotic	$x^3 + Ax + B$	2
Nonsymmetric	Short-wave	$x^2 - c_1' + c_2'$	1
Frozen field	Nonasymptotic	$x^3 + Ax + B$	2
Frozen field	Two-long-wave	$x^4 + c_1 x^2 + c_2$	2
Rapid solidification	Nonasymptotic	$x^3 + Ax + B$	2
Scaled on δ_l, δ_t	Nonasymptotic	$x^3 + Ax + B$	2

that disturbances that are smaller or *larger* than x_c are immeasurably more stable. Thus surface tension alone provides no intuition for why, near $V=V_c$ short- and long-wave dynamics will be so strongly coupled. Of course, linear theory alone provides no information about the dynamics of initially shallow cells, only the conditions that are consistent with multiple scale interactions. The point is that the cutoffs are disparate, not that surface tension is small. We see this by interpreting the cubic unfolding of Eq. (14) as follows.

Near the critical velocity, $M\sim 1$ and $\Gamma\sim 10^{-9}$, the latter varying negligibly with V. Thus, M mimics V as the bifurcation parameter near the critical velocity, and we solve for $M=M(x)$ in Eq. (14),

$$M(x)=\frac{-\alpha' x+\beta'}{x^3+A'x+B'}\ , \tag{19}$$

where $\alpha',\beta'>0$, $|A'|,B'\gg 1$, and $A'<0$, and are provided in Appendix B. This form of the bifurcation diagram reveals the structure of the standard neutral curve. The long- and short-wave cutoffs appear when Eq. (19) blows up at the two roots $x_1,x_2>0$ of the denominator. The flatness is due to the fact that $x_2-x_1\gg 1$, and $|A'|\gg 1$, the magnitude of the latter being due to that of Γ^{-1}. We can think of Γ^{-1} as the product of two ratios, $\Gamma^{-1}=[(D/V)/(\gamma_{sl}/L)](\Delta T_c/T_m)$: the ratio of the diffusion length to the capillary length, and the ratio of the equilibrium temperature difference between the planar interface and the far field to the bulk melting temperature of the planar pure solid. The size of this parameter is indeed responsible for the flatness of the curve, however, its size is not *solely* due to the surface tension, which is an intrinsic property of the material. In the materials studied, the capillary length is essentially constant, approximately an angstrom, yet the value of Γ^{-1} at the critical velocity varies by more than six orders of magnitude (see tables in [16]). This is because the diffusion length and the temperature ratio vary by at least as much among these materials. Thus, one might ascribe the flatness of the neutral curve to the long solute diffusion range. For $\Gamma^{-1}\lesssim 10^2$ wavelength selection improves substantially. When the nondimensionalization of the system of equations changes, does this qualitative behavior change?

In order to isolate the control parameters V and C_∞, Merchant and Davis [11] determined the two length and time scales remaining in the problem. These scales are $\delta_l=(\gamma_{sl}T_m/LG_L')^{1/2}$ and $\delta_t=\gamma_{sl}T_m/LG_L'D$, where all quantities are defined as previously, and the subscripts l,t denote length and time. In order for both δ_l and δ_t to be independent of V, G_L' must be independent of V. This is equivalent to the assumption that there is no curvature in the liquid temperature field near the interface, which is questionable at high solidification rates. When this assumption is valid, these scales give rise to dimensionless control variables V_{md} and C_{md} (the cursive variables in [11]) that isolate the experimental controls V and C_∞, unlike M, Γ, and of course α and β, which are combinations of the former two. The neutral surface obtained [from Eq. (2.4a) of [11]] in their formulation is also an unfolding of a cubic normal form as in Eq. (14). We expect this since a change in the length and time scales should not change the singular behavior of the eigenvalue problem for the solidification system. This formulation exhibits weak wavelength selection near the critical bifurcation point [11], which is qualitatively similar to that exhibited in the standard scales of Eq. (19). When transforming into their variables $M=V_{md}C_{md}(1+n)/(2+l_{md}V_{md})$ and $\Gamma=V_{md}/C_{md}$, in the limit of small V_{md}, an equation for $V_{md}(x)$ with the same structure as Eq. (19) is obtained. In this case, it is the magnitude of C_{md} that is responsible for the flatness of the curve. C_{md} can be large due to a small liquid temperature gradient, melting point, segregation coefficient, and surface tension, or due to large latent heat, solute concentration, or liquidus slope. Two of these variables are true experimental controls. The point is that while the selection problem is made worse by the smallness of interfacial surface tension, it is not entirely dependent on the material, or the scaling of the solidification system. Rather, it is caused by the nature of the singularity at the critical velocity, the magnitude of the linear coefficient of the cubic unfolding, and other intrinsic properties of the formulation.

IV. DISCUSSION

We performed an equivalence transformation of the bifurcation problem for g to one that is an unfolding of a cuspoid normal form $N=x^3$. When viewed as a two-parameter unfolding of N, the neutral surface is the folded cusp surface which arises in the study of a variety of physical systems [12,14,15]. This is shown in Fig. 3. The solution of the solidification problem is tantamount to solving the bifurcation problem for the one-parameter unfolding of N, Eq. (14), which results in a neutral path F in the neutral surface F_2. There are an infinite set of *degenerate points* of the unfolding f_2, which form the *bifurcation set* S defined by a semicubical parabola [Eq. (16)]. Along S the nature and number of the real solutions to Eq. (15) change (Fig. 3). A neutral stability plane is drawn in terms of control variables by projecting the surface F_2 and $F\cap F_2$ onto the plane $T(A,B)$ (Fig. 4). We showed that if the neutral path enters and exits the right-hand nappe S_1 of the bifurcation set S, then the neutral curve will be closed. The manner in which the path F intersects S will determine the strength of the wavelength selection. This depends on the sensitivity of the unfolding parameters to the underlying control, and on the degree m of the normal form. Examples of two different open curves and a closed curve that result from three paths through S are given in Fig. 5. By slicing $F\cap F_2$, we drew the $|\alpha|$-x and β-x neutral curves, the former being is relatively sharper close to the critical velocity. These are shown in Fig. 6. While selection is sharpened, this is merely a surgical bypass of the problem since these are not strictly experimental controls.

We interpreted F_2 as the catastrophe manifold of a potential function Φ, that is the universal unfolding (with respect to right equivalence) of a quartic cuspoid. Minimizing Φ provides the equilibria that form a neutral

surface the same as that in Fig. 3. The equilibria of Φ vary as the controls A,B vary. For A,B such that $|1-V/V_c| \ll 1$, we found that, with respect to imperfections in V, the critical points V_c and V_a are structurally unstable as critical points.

Once the results of a linear theory are cast in the form of Eq. (14), an entire rostrum of rich mathematical tools is made available [12,14,15], simplifying studies of different solidification models. The inclusion or exclusion of L does not change the codimension of the unfolding. Rather, only the dependence of the unfolding parameters on the bifurcation parameter changes. In some asymptotic limits (Sec. III C), the relevant unfolding will be of a different normal form, and the behavior of $F \cap F_2$ will be replaced by new singular behavior. This suggests an investigation of new asymptotic theories using normal form analysis. We have shown that four solidification models have the same singular behavior, but that asymptotic limits do not. The distinctions are cataloged in Table I. Higher-order singularities may occur in models that have not been studied here. The significance of thinking about the problem in this manner is that the nature and number of singularities characterize the topological structure of the particular solidification system. As in the case of two state variables [15], the anatomy of the problem can be characterized by the singularities, and one can ask, "When are two solidification systems similar?" The answer depends on the codimension of the unfolding of the cuspoid.

V. CONCLUSION

We have studied the qualitative behavior of the neutral modes of four solidification models. By exploiting the techniques of catastrophe, singularity, and bifurcation theories, several interesting features of the equations are observed.

(i) The steady modes of these models are described by a cusp manifold that is an unfolding of a cubic normal form. Certain short- and long-wave asymptotic limits of the models are described by unfoldings of quadratic and quartic normal forms. This bounds the number of critical points of the models between one and three.

(ii) The number and type of singularities is invariant to scale changes, and the addition of a number of physical features to the basic solidification model.

(iii) The cusp manifold can be derived as the singularity set of a quartic normal form, in which the critical points of the system are unstable to experimental imperfections. In two long-wave limits the unfolding is quartic, suggesting that slow mode behavior may be difficult to verify experimentally.

(iv) The initial bifurcation point occurs on a part of the upper fold that has minimal curvature, exhibiting the topological origin of weak wavelength selection. We find that the flatness of the neutral curve is an artifact of the material and control parameters *and* the normal form characteristic of the formulation.

We point to the simplicity and limited number of singular events as a diagnostic of the utility of the approach. These methods equip us with simple criteria to determine when two solidification formulations are similar. For example, it is known that direct comparisons of the one-sided and symmetric formulations, lead to ambiguous conclusions [5]. Thinking of the problem topologically allows us to define the difference between formulations, based on the degree of the cuspoid, and the codimension of the unfolding. The suggestion is that two models are fundamentally similar if the number and type of their singularities do not differ. Therefore, complex differences between results of various formulations can be studied geometrically.

ACKNOWLEDGMENTS

Conversations with A. S. Thorndike, P. D. Mourad, R. Colony, and G. J. Merchant have been most helpful. This work has been supported by the Office of Naval Research under Grant No. N00014-90-J-1227 and the Applied Physics Laboratory, University of Washington.

APPENDIX A

We collect here the similarities between catastrophe, singularity, and bifurcation theories that are relevant to the problem as discussed in Sec. III. A complete discussion can be found elsewhere [12]. For systems with n state variables, the distinction between these theories is clear; however, when $n=1$, they are similar.

In catastrophe theory one studies the structure of the critical points of real valued functions f in E^n. In singularity theory one studies the structure of the zeros of mappings h: $\mathbb{R}^n \to \mathbb{R}^n$. In bifurcation theory one studies the structure of the zeros of mappings g: $\mathbb{R}^n \times \mathbb{R} \to \mathbb{R}^n$, which depend on a distinguished parameter. Since the critical points of f are determined by finding the zeros of the mapping $h=\nabla f$, and bifurcation problems g are just one parameter families of mappings h, the existence of a relation between the theories should not be surprising [12]. It is the notion of equivalence that sets the distinction.

The manner in which two functions are defined to be *equivalent* differs as follows. In catastrophe theory, two functions f_1 and f_2 in E^x are *right equivalent* if there exists a diffeomorphism germ $X(x)$ with $X(0)=0$ and a constant satisfying $f_1(x)=f_2(X(x))+\text{const}$. In singularity theory, two mappings h_1 and h_2 are *contact equivalent* if there exists a diffeomorphism germ $X(x)$ with $X(0)=0$ and a nonsingular $n \times n$ matrix $M(x)$, depending smoothly on x such that $h_1(x)=M(x)h_2(X(x))$. Contact equivalence for bifurcation problems is a one-parameter version of the above.

While these differences exist, the structure of unfolding theory is identical among the approaches. When there is a single state variable $n=1$, the functions f become $f:\mathbb{R} \to \mathbb{R}$, and the mappings h become $h:\mathbb{R} \to \mathbb{R}$. Given a cuspoid normal form $\pm x^m$, for some m, each function $f(x)$, of finite codimension, is right equivalent to it. Similarly, each mapping $h(x)$, of finite codimension, is contact equivalent to this cuspoid. In addition, the unfoldings in these categories are simply related as follows.

The normal forms x^{m+1} and x^m, have codimension $m-1$ in catastrophe and singularity theories, respectively. A universal unfolding of x^{m+1} with respect to right equivalence is

$$G(x,A)=x^{m+1}+A_{m-1}x^{m-1}+\cdots+A_1x \ . \quad \text{(A1)}$$

A universal unfolding of x^m with respect to contact equivalence is

$$H(x,B)=x^m+B_{m-2}x^{m-2}+\cdots+B_1x+B_0 \ , \quad \text{(A2)}$$

which, up to rescaling parameters, obtains upon differentiation of the unfolding with respect to right equivalence. The choice of $m=3$ connects G and H to Φ and f_2 of Sec. III. The pictures of catastrophe theory, determined from $\partial_x G=0$, are identical to those of singularity theory, determined by solving $H=0$. So that for the case of a single state variable and finite codimension, the generating functions of catastrophe theory can be unambiguously constructed from the mappings of singularity theory.

APPENDIX B

We record here the coefficients and the unfolding parameters of the various solidification models and asymptotic limits discussed in Sec. III, and summarized in Table I. The coefficients that appear in Eq. (19) are

$$\alpha'=\Gamma^{-1} \ , \quad \text{(B1)}$$

$$\beta'=\frac{\Gamma^{-1}}{3}(2k-1)>0 \ \text{ for } k<0.5 \ , \quad \text{(B2)}$$

$$A'=k-\Gamma^{-1}-\frac{(k+1)^2}{3} \ , \quad \text{(B3)}$$

$$B'=(k-\Gamma^{-1})\frac{k+1}{3}+\frac{2}{27}(k+1)^3 \ . \quad \text{(B4)}$$

(i) The unfolding parameters of the nonsymmetric model, as derived in Sec. II, can be obtained by inspection from Eqs. (12) and (13).

(a) The nonsymmetric short-wave limit $a^2\gg 1\gg k$. The unfolding parameters appearing in Eq. (18) and Table I, with $x=a$, are

$$c_1'=\Gamma^{-1}, \quad c_2'=M\Gamma^{-1} \ . \quad \text{(B5)}$$

(ii) Although the characteristic equations of the frozen-field and nonsymmetric models differ substantially, the unfolding parameters are identical in form. However, their functional dependence on the primary bifurcation parameter V is different because in the frozen-field model the liquid temperature gradient is independent of V. [See the discussion following Eq. (10) and the form of G^* following Eq. (2).]

(a) The frozen-field long-wave limit $k\ll a^2\ll 1$, near the critical velocity [13]. The unfolding parameters appearing in Eq. (17) and Table I, with $x=a$, are

$$c_1=\Gamma^{-1}(1-M^{-1}), \quad c_2=k\Gamma^{-1} \ . \quad \text{(B6)}$$

(b) The frozen-field long-wave limit $a^2\ll 1\sim k$, near absolute stability [13]. The unfolding parameters appearing in Eq. (17) and Table I, with $x=a$, are

$$c_1=\frac{k\Gamma-1}{1/k+1}, \quad c_2=k\frac{M^{-1}}{1/k+1} \ . \quad \text{(B7)}$$

In the case of the cubic unfolding x^3+Ax+B, we present the parameters p,q,r from the cubic R^3+pR^2+qR+r, where $x-p/3=R$, and

$$A=q-\frac{p^2}{3}, \quad B=\tfrac{1}{27}(2p^3-9pq+27r) \ . \quad \text{(B8)}$$

(iii) The nonasymptotic unfolding of the model of rapid solidification [7] has unfolding parameters A,B as in Eq. (B8), with

$$p=2-\bar{k} \ , \quad \text{(B9)}$$

$$q=\Gamma^{-1}[\Gamma(1-\bar{k})-(M^{-1}+\tilde{k})] \ , \quad \text{(B10)}$$

$$r=\Gamma^{-1}[(\bar{k}-1)(M^{-1}+\tilde{k})-\hat{k}] \ , \quad \text{(B11)}$$

where $x-p/3=R$, and $R=-(\frac{1}{4}+a^2)^{1/2}-\frac{1}{2}=\lambda_1$ of [7(b)]. Here, $\bar{k}=k(v=1)$, where $v=(1+h_t)(1+h_x^2)^{-1/2}$ is the local interface speed and

$$\tilde{k}=\frac{k_E\tilde{m}(1)}{k_E+\beta}, \quad \hat{k}=\frac{k_E\tilde{m}(1)}{1+\beta} \ ,$$

k_E is the equilibrium segregation coefficient, $k(v=0)$, and β is an interfacial kinetics parameter as defined in [7]. In addition,

$$\tilde{k}=\frac{k_E\tilde{m}(1)}{k_E+\beta}, \quad \hat{k}=\frac{k_E\tilde{m}(1)}{1+\beta} \ ,$$

where $\tilde{m}(1)$ relates the equilibrium segregation coefficient to $k(v)$, at $v=1$, and its functional form is given in Ref. [7].

(iv) The nonasymptotic unfolding of the model based on length and time scales δ_l and δ_t [11] has unfolding parameters A,B as in Eq. (B8), with

$$p=kV_{md} \ , \quad \text{(B12)}$$

$$q=\frac{2+l_{md}V_{md}}{(1+n)}-C_{md}V_{md}+V_{md}^2(k-1) \ , \quad \text{(B13)}$$

$$r=V_{md}\left[\frac{2+l_{md}V_{md}}{(1+n)}(k-1)+C_{md}V_{md}\right] \ , \quad \text{(B14)}$$

where $x-p/3=R=\lambda_1$ of [11], and $R^2-V_{md}R=a^2$.

[1] D. J. Wollkind and L. A. Segal, Philos. Trans. R. Soc. London **268**, 351 (1970).

[2] W. W. Mullins and R. F. Sekerka, J. Appl. Phys. **35**, 444 (1964).

[3] J. S. Langer, Rev. Mod. Phys. **52**, 1 (1980); and in *Chance and Matter,* edited by J. Souletie, J. Vannimenus, and R. Stora (North-Holland, New York, 1987).

[4] P. Haug, Phys. Rev. A **35**, 4364 (1987); **40**, 7253 (1989).

[5] A. Karma and P. Pelcé, Phys. Rev. A **44**, 1419 (1991).
[6] M. J. Bennett and R. A. Brown, Phys. Rev. B **39**, 11 705 (1989).
[7] (a) G. J. Merchant and S. H. Davis, Acta Metall. **38**, 2683 (1990); (b) R. J. Braun and S. H. Davis, J. Cryst. Growth **112**, 670 (1991).
[8] J. I. D. Alexander, D. J. Wollkind, and R. F. Sekerka, J. Cryst. Growth. **79**, 849 (1986).
[9] S. R. Coriell, G. B. McFadden, and R. F. Sekerka, Annu. Rev. Mater. Sci. **15**, 119 (1985).
[10] J. S. Wettlaufer, Europhys. Lett. **19**, 337 (1992).
[11] G. J. Merchant and S. H. Davis, Phys. Rev. B **40**, 11 140 (1989).
[12] M. Golubitsky and D. Schaeffer, *Singularities and Groups in Bifurcation Theory* (Springer, New York, 1985), Vols. I and II; also see Appendix A in this paper.
[13] D. S. Riley and S. H. Davis, SIAM J. Appl. Math. **50**, 420 (1990); G. I. Sivashinsky, Physica D **8**, 243 (1983); K. Brattkus and S. H. Davis, Phys. Rev. B **38**, 11 452 (1988).
[14] T. Poston and I. Stewart, *Catastrophe Theory and its Applications* (Pitman, Boston, 1978).
[15] A. S. Thorndike, C. R. Cooley, and J. F. Nye, J. Phys. A **11**, 1455 (1978).
[16] S. De Cheveigné, C. Guthmann, P. Kurowski, E. Vicente, and H. Biloni, J. Cryst. Growth **92**, 616 (1988).

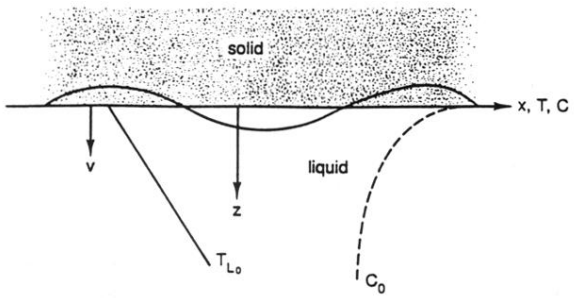

FIG. 1. Schematic of the solidification system in which the phase boundary is moving downward into the liquid. The steady-state thermal T_{L0} and concentration C_0 fields are represented, and there are no horizontal boundaries.

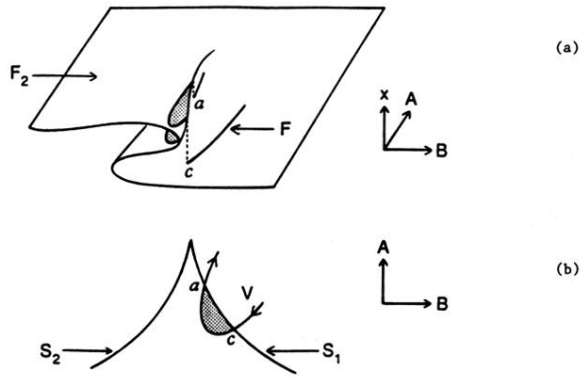

FIG. 4. (a) The *neutral path* F in the surface F_2. The path "begins" on the lower right-hand sheet of F_2 where the solutions are unphysical. The path "jumps" up to the right-hand fold [see (a)] or crosses the right-hand nappe of the *bifurcation set* S_1 [see (b)] when $(A,B)=(\alpha_c,\beta_c)$, labeled by c. The system stabilizes after exiting the cusp region [see (b)] at $(A,B)=(\alpha_a,\beta_a)$, labeled by a. The shaded area is the region of instability. The path is parametrized by the underlying bifurcation parameter V, and C_∞ is fixed at the value in Fig. 2. A neutral curve is closed if the path F enters and exits S by crossing S_1.

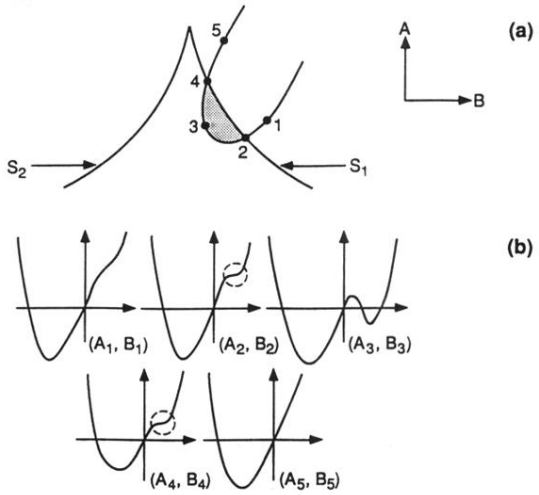

FIG. 7. (a) Five points (A_i,B_i) in F. (b) The graph of $\Phi(x, A,B)$, an unfolding (with respect to right equivalence [12]) of the cuspoid normal form x^4 for these five points. We are particularly interested in the structure of the critical points. Notice (dashed circle) that at the points (A_2,B_2) and (A_4,B_4), the function Φ has locally cubic inflections. These singularities correspond to velocities V_c and V_a, and are structurally unstable as critical points, and the equilibria of Φ form the surface F_2 in Fig. 3 (see text).